Simulating the sub-barrier nuclear fusion of ^{144}Sm and ^{16}O using a single barrier wave packet model

Student 6625008[1]

[1]School of Mathematics and Physics, University of Surrey

I investigated the single barrier model theoretical framework for describing low energy fusion scenarios by simulating a head-on collision between ^{16}O and ^{144}Sm and determining the probability of fusion. Implementing an explicit forward Euler finite difference approximation enables the time dependent Schrödinger equation to be numerically solved for a single spatial dimension, one body system. Utilising a Gaussian wave packet initial wavefunction, a systematic study is conducted over a parameter space characterized by varying the initial Gaussian spatial width and its initial mean energy. The time dependent numerical transmission probabilities were found to tend to the analytical and time independent Schrödinger equation comparison solutions. However, a consistent lack of agreement arises due to the simulated wave packets non-zero energy variance, which does not reproduce the expected dirac-delta function like energy distribution seen within experiments. A literature review of the single barrier model exhibits the inadequacy of the model to accurately reproduce experimental results and motivates the use of a coupled channels paradigm to describe the low energy fusion mechanism. The versatile Gaussian wave packet approach, for representing the projectile-target relative motion's wavefunction, should be combined with energy projection techniques and coupled channel fusion schemes, to extend this investigation into low energy nuclear fusion, and, explore further dynamics of such nuclear fusion systems.

Supervisor: Dr. Alexis Diaz Torres

Contents

1 Introduction

Nuclear fusion has been a long researched area of atomic and quantum physics on account of it emerging just under a century ago with a notable publication providing the first calculations estimating the rate of nuclear fusion within stars [1]. Understanding the physics behind fusion in various systems has seen great interest and extensive research efforts over the course of the 20th century, due to its fundamental role in stellar processes and nucleosynthesis. As a result of this, the field has expanded and has subsequently found a variety of applications: within weapons of mass destruction, the first such weapon being the Ivy Mike device [2], or the ongoing development of a fusion based energy source such as the International Thermonuclear Fusion Reactor (ITER)[3]. Importantly, nuclear fusion of complex nuclei at very low energies involves the one of the most important consequences of quantum mechanics, the process of quantum tunneling [4]. In these systems, incoming nuclei have insufficient energy to overcome the repulsive Coulomb barrier and fuse with the target nuclei, instead being scattered away. However, quantum mechanics allows for an incoming nuclei of insufficient energy to 'tunnel' through this barrier, which would classically be impassable, allowing it to fuse with the target. The importance of such systems and the ability to understand the mechanisms and underlying structures cannot be understated: "Quantum tunneling in systems with many degrees of freedom is one of the fundamental problems in physics and chemistry" [5].

A theoretical framework that describes the fusion process traces its origins to Bethe's publications on explaining energy production in stellar bodies [6]. Throughout the 1940s and 1950s, research into the underlying physics of fusion was carried out for three key purposes: to develop military weaponry, to create fusion powered energy sources, and to improve astronomical theories. It is important to note that fusion reactions take many forms due to a variety of conditions and variables that can effect the process e.g. at energies much larger than the Coulomb barrier energy dissipation effects must be considered [7, 8]. Of great interest and which is the focus of my report, is the nuclear fusion of complex heavy nuclei around and below the height of the Coulomb barrier. Developments in nuclear physics throughout the 1940s and 1950s gradually grew the fusion theoretical framework, incorporating new physics such as the Woods-Saxon nuclear potential [9], overall giving rise to a general 'single barrier model' to explain low energy heavy nuclei fusion reactions. Analysing in one dimension, the core premise of this model is characterized by a long-range repulsive Coulomb, and short-range attractive nuclear Woods-Saxon, interaction between a projectile and target nuclei pair. The interaction yields a potential barrier, commonly referred to as the Coulomb barrier, followed by a potential trough within the nuclear radius of the target nuclei. The model assumes that if a projectile nuclei occupies the potential pocket it is absorbed into the fusion channel and fusion occurs.

Analytical formula describing fusion, such as the Hill-Wheeler formula, emerged allowing for theoretical calculations of the reactions nuclear cross section, which importantly, is an experimentally measurable quantity [10]. The shape and location of the Coulomb barrier is described by a set of parameters which were then adjusted to fit to experimental cross section data [11]. However, mirroring drawbacks in fusion energy research, the technology of the mid-twentieth century was not able to support the advances and explore the concepts, with sufficient quantities and precise nuclear cross section data being inaccessible. Consequently, the established single barrier model saw little challenge until the 1980s with improved experimental nuclear cross section data. Several experiments saw that sub-barrier fusion cross section data, for intermediate mass systems, was found to be significantly larger than the predicted by the single barrier model [12]. Further analysis by inversion of experimental data was used to determine an effective potential which also disagreed with the model [13]. These contradictions between theory and experiment motivated the formulation of an improved framework to describe low energy sub-barrier fusion supported by improving experimental results through the 1980s and early 1990s [14]. The revised theoretical framework for fusion replaced the simplistic 'single barrier to overcome' approach with a more comprehensive model, encompassing and accounting for the complexity of fusion reactions. The 'coupled channel' formalism recognizes the coupling of different reaction channels giving rise to enhanced fusion cross sections e.g. coupling between the translational motion and internal degrees of freedom, e.g. intrinsic rotation and/or vibration of the nuclei. The coupled channel formalism has developed in the three decades since

its inception, but it remains the current working framework for fusion and is still subject to advancement today.

To investigate the the single barrier model, I created a programme from scratch to simulate a dynamic fusion reaction between ^{16}O and ^{144}Sm. To explore such a dynamic quantum system, I exploited the Time Dependant Schrödinger Equation (TDSE) to achieve a numerical simulation. The $^{16}O + ^{144}Sm$ reaction provides a strong avenue of study when attempting to analyse the impact of collective vibrational states of the target nuclei on the fusion cross section [15]. Hence, it is one of the many repeated reactions highlighted within the literature, and a wealth of experimental results are available for the reaction [16]. However, analysing impact of collective vibrational states of the target nuclei is outside the scope of this report and will not be further considered. The focus of my investigation is a head-on collision between the reactants, characterized as an s-wave or $\ell = 0$ collision, simplifying the calculations and computational requirements. To further simplify, and a standard practice in fusion investigations, symmetry allows for a reduction to a single spatial dimension denoted by r. Additionally, the two body collision is reduced to a single body problem by analysing the scattering reaction in the center-of-mass frame. I utilise an explicit finite difference approximation for the first and second order derivatives to transform the TDSE. With considerations of the boundary conditions and system dynamics, a Gaussian Wave Packet (GWP) wavefunction is exercised as an ansatz, to represent the radial motion of the $^{16}O - ^{144}Sm$ reduced mass, a choice which is supported by similar investigations with GWP trial wavefunctions [17, 18, 19, 20]. To simulate the irreversible fusion of the target and projectile nuclei into a compound nucleus, and to incorporate other unaccounted for degrees of freedom, an imaginary absorption potential is implemented. The Hamiltonian operator $\hat{H}$ in the TDSE is a unitary operator defined by $\hat{H}^{\dagger}\hat{H} = \mathbb{I}$. With a unitary propagator, the quantum evolution of the wavefunction becomes deterministic and reversible with no information loss, as the system evolves in time, so long as quantum coherence is maintained. Adding the complex absorption potential, the Hamiltonian operator now becomes non-Hermitian. This complex potential acts specifically within the Coulomb barrier to 'capture' any of propagated GWP wavefunction which overcomes or penetrates the barrier. This reaction occurs on the zeptosecond timescale (1 zs $= 10^{-21}$ s), ensuring quantum coherence is maintained, such that after the GWP interacts with the Coulomb barrier, any wavefunction probability density within the pocket is absorbed via the absorption potential and their is a reduction in the overall normalisation of the wavefunction. This loss of normalisation will be used to quantify the probability of a projectile ^{16}O nuclei transmitting through the barrier and fusing with the ^{144}Sm target nuclei. After a thorough literature review, I individually created and coded the programme used for my investigation.

The layout of the report is as follows: Section 2 sets up the single barrier model for fusion for a $^{144}Sm + ^{16}O$ reaction, exploring important analytical formula and physics with comparisons to experimental data. Section 3 details the numerical tools, programme features and methods for extracting useful results from the simulations. Section 4 analyses the collective simulation results and scrutinizes the models and methods used. Finally, Section 5 summaries and presents the conclusions of my investigation.

2 Theory

2.1 Single Barrier Fusion Model

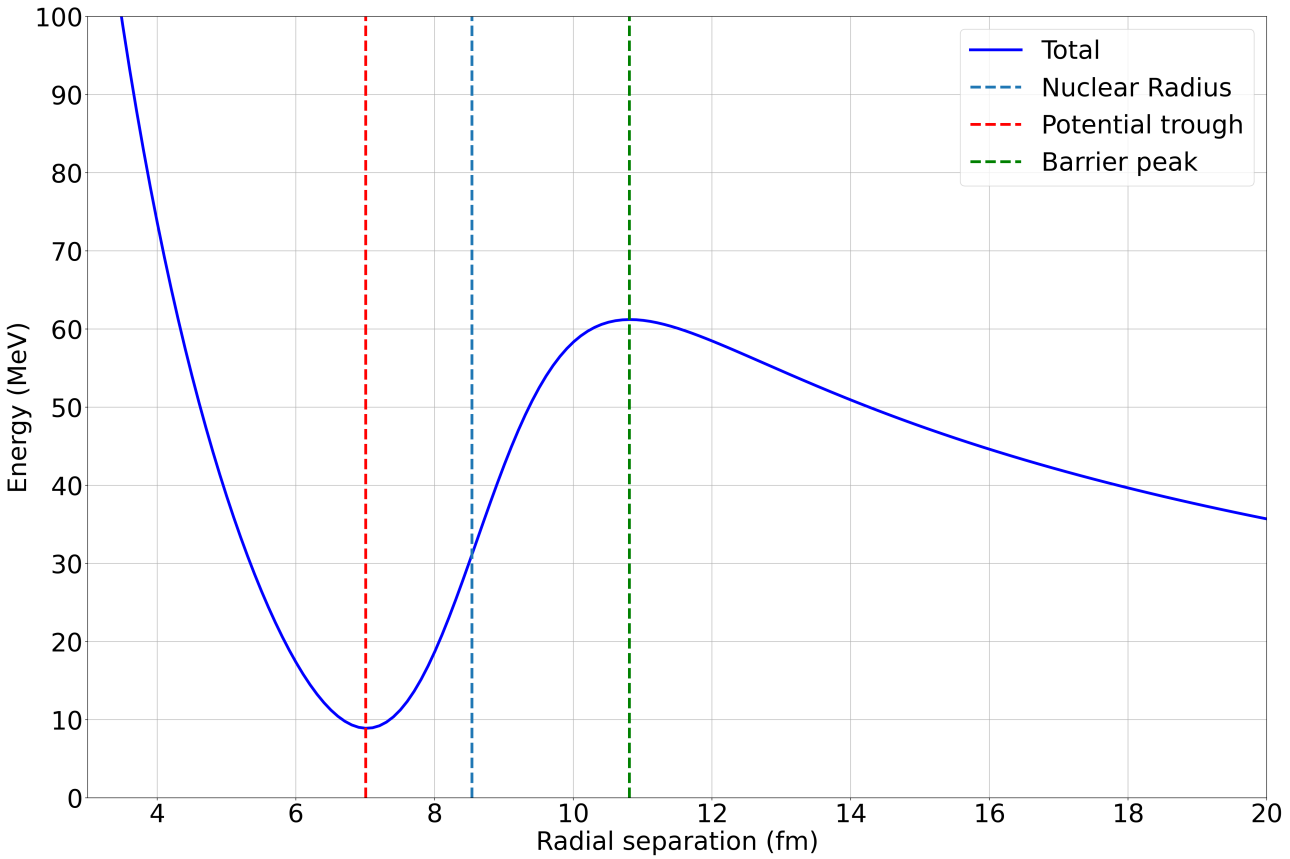

Figure 1: Total real potential (equation 1) for a $\ell = 0$ $^{144}Sm + ^{16}O$ fusion scenario. Dark blue dashed line indicates the nuclear radius R used in the Woods-Saxon potential. Red dashed line indicates the minimum potential within the Coulomb barrier. Green dashed line indicates the maximum height of the Coulomb barrier B.

The total potential of the system is given by,

$$V_\ell(r) = V_N(r) + V_C(r) + \frac{\hbar^2 \ell(\ell+1)}{2\mu r^2}, \tag{1}$$

where ℓ is the orbital angular momentum, r is the radial separation of the two nuclei and the reduced mass of the system is given by,

$$\mu = \left(\frac{A_P A_T}{A_P + A_T}\right) m_u, \tag{2}$$

where A_P and A_T are the projectile and target's respective nucleon numbers, with m_u being the Atomic Mass Unit. $V_N(r)$ gives the short-range attractive Woods-Saxon potential of the form,

$$V_N(r) = -\frac{V_{WS}}{1 + \exp\left[\frac{r-R}{a_{WS}}\right]}, \tag{3}$$

with V_{WS} being the depth of the Woods saxon potential, $R = r_{WS}(A_P^{1/3} + A_T^{1/3})$ is the nuclear radius with r_{WS} being the well center factor, and a_{WS} is the well diffuseness parameter. The Coulomb potential is given by,

$$V_C(r) = \frac{Z_P Z_T e^2}{r}, \tag{4}$$

with Z_P and Z_T being the respective charge numbers and e is the elementary charge.

The crux of the single barrier model lies within the existence of this clear potential barrier seen in Fig. 1. A simple criterion arises for two colliding nuclei to fuse together: if the target nuclei surpasses the Coulomb barrier and enters the potential well, the nuclei will fuse. Therefore, to investigate the fusion of two nuclei, the natural next step is to look at how the colliding nuclei can get into this potential well and how likely is that to happen.

2.2 Transmission Probability

To determine the probability of fusion for the projectile-target system described by the potential above, it is necessary to analyse the Coulomb barrier and importantly, assess the transmission through this barrier at energies above and below the barrier height, including quantum tunneling effects. As such, it is standard to assume the system potential is parabolic in the vicinity the Coulomb barrier. From this approximation, the probability of transmission through a parabolic barrier can be calculated as,

$$T_\ell(E) = \left(1+\exp\left[\frac{2\pi}{\hbar\omega}\left(B-E+\frac{\hbar^2\ell(\ell+1)}{2\mu R^2(E)}\right)\right]\right)^{-1}. \tag{5}$$

This is known as the Hiller-Wheeler formula [10] which has been modified to include the centrifugal momentum term[15]. B is the height of the parabolic Coulomb barrier and $R(E)$ is the effective radius which was found to be a slowly varying function in E and is typically replaced by the radius of the $\ell = 0$ or s-wave barrier peak r_0, this is further elaborated on in section 2.4. Lastly, $\hbar\omega$ is the curvature of the barrier calculated using,

$$\hbar\omega = \sqrt{\frac{\hbar^2}{\mu}\frac{d^2V(r_0)}{dr^2}}, \tag{6}$$

where the second derivative of the potential with respect to position is evaluated at the $\ell = 0$ peak barrier radius. This investigation focuses upon a head on a collision between the two nuclei with $\ell = 0$, enabling a transformation of (5) to,

$$T_0(E) = \left(1+\exp\left[-\frac{2\pi}{\hbar\omega}(E-B)\right]\right)^{-1}. \tag{7}$$

This expression for the transmission probabilities is accurate for energies near B, the height of the Coulomb barrier, but fails at much lower energies as the parabolic approximation breaks down [5].

2.3 Fusion Cross Section

The nuclear cross section of a fusion reaction is a very useful quantity with it being experimentally measurable and can be used to confirm or contest theory on the underlying physics of fusion processes. The total nuclear cross section is found as a function of energy and given by a infinite summation over partial waves,

$$\sigma(E) = \sum_0^\infty \frac{\pi\hbar^2}{2\mu E}(2\ell+1)T_\ell(E), \tag{8}$$

with the $\ell = 0$ barrier nuclear cross section given by

$$\sigma_0(E) = \frac{\pi\hbar^2}{2\mu E}T_0(E). \tag{9}$$

Extending the parabolic approximation of the Coulomb barrier, an analytical formula can be found for the fusion cross section commonly known as the Wong formula [21],

$$\sigma(E) = \frac{\hbar\omega R^2(E)}{2E}\ln\left(1+\exp\left[\frac{2\pi}{\hbar\omega}(E-B)\right]\right). \tag{10}$$

A comparison of the analytical Wong formula to experimental data is presented in Fig. 2. Whilst Wong's formula does replicate the experimental results at super-barrier energies, the formula underestimates the fusion cross section at sub-barrier energies, raising doubt in the viability of the single barrier model for fusion.

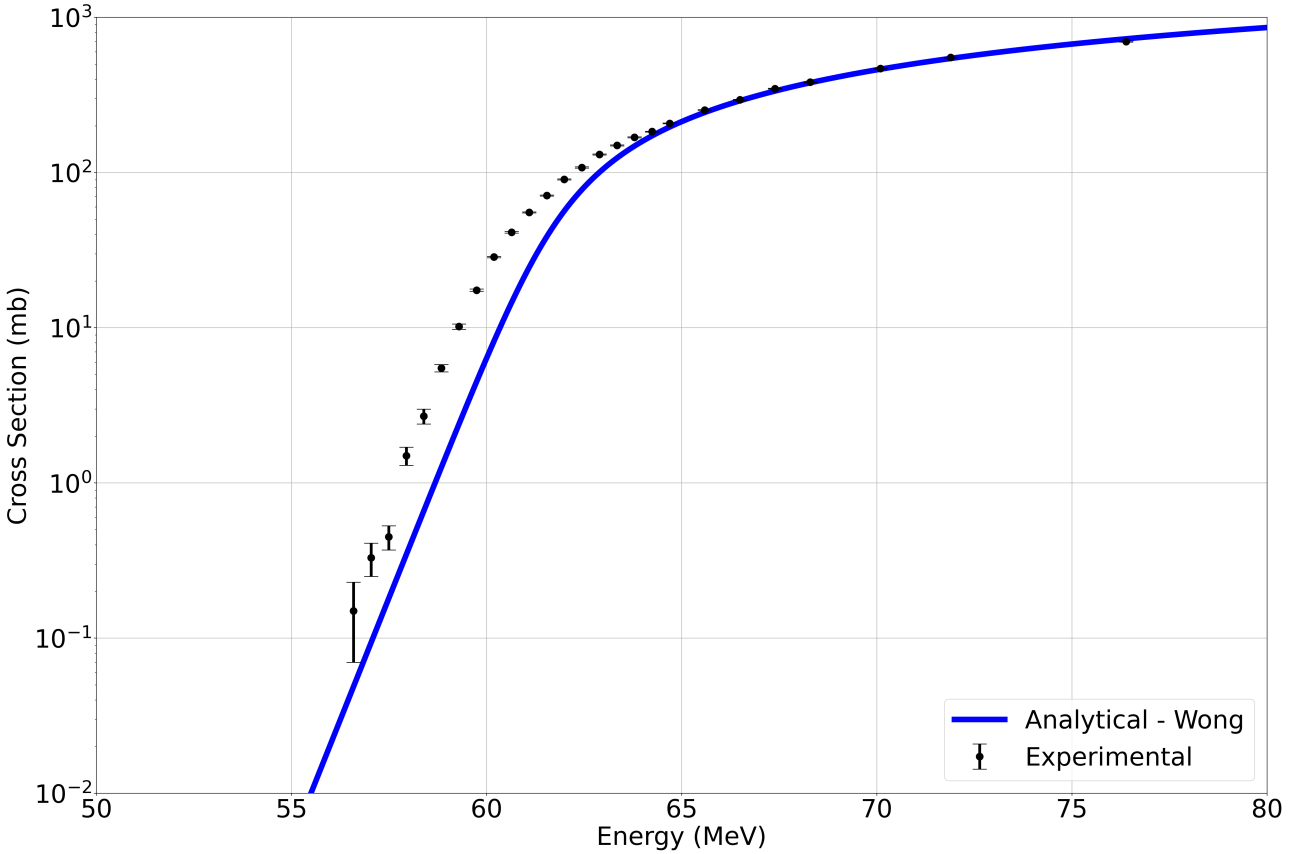

Figure 2: Nuclear fusion cross section for a $\ell = 0$ $^{144}Sm + ^{16}O$ fusion scenario. Black: Experimental data with error bars [16]. Blue: Wong's analytical formula (equation 10).

2.4 Analytical Barrier Distributions

The exact mechanisms which govern the fusion process have been shown to be more complicated than once proposed, and is an active and ongoing area of physics research. The interacting nuclei exhibit a variety of properties and dynamics, which feed into the fusion process, and discredit the simplistic idea of a single barrier to overcome, to achieve fusion. [22]. The properties manifest into couplings between various reaction channels e.g. elastic, inelastic, scattering, transfer, break-up and fusion reactions, this is the aforementioned coupled channel formalism. Such variety gives rise a 'distribution of barriers' which more accurately depicts the physics and describes the fusion process [23]. Extensive research into quantifying the distribution of barriers for fusion reactions and extracting them from experimentally available data has been conducted (non-exhaustive list) [15, 16, 24]. Various different mathematical approaches can be used to find a fusion barrier distribution, which typically start by defining,

$$E\sigma(E) = \pi R^2(E) \sum_{\alpha} w_\alpha (E - B_\alpha), \tag{11}$$

where w_α is the barrier weight and B_α is the barrier height with an associated channel index α corresponding to a given barrier [16]. Interpreting this equation classically, one would see sets of delta functions across a range of energies near the Coulomb barrier energy ($E = B_\alpha$), specifically, peaks occurring in the nuclear fusion cross section $\sigma(E)$ due to the existence of a barrier α enhancing the cross section and subsequently facilitating the fusion process. Calculating $d^2(E\sigma)/dE^2$ will return back the original delta functions and you can see a 'distribution of barriers' at specific energies. However, invoking a quantum mechanical interpretation and including quantum tunneling considerations, a smooth variation in the nuclear fusion cross section in the proximity of a given barrier will be obtained. Calculating $d^2(E\sigma)/dE^2$ now will instead produce a continuous function in complete contradiction to classical conventions, and can provide insights into the existence of additional barriers and coupling, that occurs within the fusion reactions [5, 16]. It is salient to note here, that within the literature surrounding this topic, there is a significant lack of clarification on the exact quantity which defines and is the,

distribution of barriers. Specifically, some define a continuous distribution function $D(E) = \frac{1}{\pi R^2(E)} \frac{d^2(E\sigma)}{dE^2}$ as the barrier distribution [15]. Whereas others define $\frac{d^2(E\sigma)}{dE^2}$ as the barrier distribution [5]. Irrespective of convention, they conceptually represent the same quantity, and so, henceforth, I will refer to the distribution of barriers as the latter definition of $\frac{d^2(E\sigma)}{dE^2}$.

An analytical expression for the distribution of barriers can be found as,

$$\frac{d^2(E\sigma(E))}{dE^2} \sim \pi R^2(E) \left(\frac{dT_0(E)}{dE} \right) + O\left(\frac{dR(E)}{dE} \right). \tag{12}$$

Using the analytical s-wave transmission probability from equation (7), one can ascertain a purely analytic expression for the distribution of barriers for a given fusion reaction.

The final term in equation (12) encapsulates an associated error arising due to the variation in $R(E)$. An analysis into the energy dependance of the effective radius $R(E)$ has been carried out to assess the impact of $O(\frac{dR}{dE})$ on the distribution of barriers. As a result of $R(E)$, the position and weight of the barrier peaks could vary, or a multiplicative factor could create a significant disconnect between experimental and analytical barrier distributions. However, assessing further, it was found that due to the slow variation of $R(E)$ in E, these effects would be drastically minimised. Consequently, the final term in equation (12) becomes omissible, and the effective radius $R(E)$ can be sufficiently approximated to the radius of the s-wave barrier, r_0 [5].

2.5 Experimental Barrier Distributions

The distribution of barriers can be extracted from a data set of extrapolated nuclear cross sections using the finite difference formula,

$$\frac{d^2(E\sigma)_i}{dE^2} = \left(\frac{(E\sigma)_{i+1} - 2(E\sigma)_i + (E\sigma)_{i-1}}{\Delta E^2} \right). \tag{13}$$

The associated statistical error for the second derivative evaluated at $(E\sigma)_i$ is approximated as,

$$\delta_c \simeq \left(\frac{E}{\Delta E^2} \right) \left[(\delta\sigma)_1^2 + 4(\delta\sigma)_2^2 + (\delta\sigma)_3^2 \right]^{1/2}, \tag{14}$$

where $(\delta\sigma)_i$ are absolute errors [15]. Common practice is to measure σ with a fixed percentage error, being proportional to σ and energy. As such, barrier distributions extracted using (13), will be well defined at the lower energies with a large percentage error (δ_c), and worse at higher energies with a smaller percentage error. (δ_c) is proportional to the inverse of ΔE^2, so extracting distributions over larger energy intervals smooths the function and reduces the associated error. However, this smoothing can dampen features of the distribution if the step size is smaller than the energy scale. The distribution is already smoothed by $0.56\hbar\omega$ because of quantum tunneling. Choosing a step size of $\Delta E \approx 2MeV$ does not add significant additional smoothing and will maximise the reduction in uncertainty.

Exploring the distribution of barriers in Fig. 3, a clear disparity can be seen between the single barrier analytical formula and the experimentally calculated distribution of barriers. Importantly, the presence of a smaller peak in the distribution, disconnected from the main large barrier peak centered around the B, indicates that the single barrier model does not encapsulate all the physics and processes which factor into the fusion reaction. The barrier distribution divergence further discredits the validity of the single barrier model for its inability to replicate the additional barriers and enhancements in the fusion cross section seen in the experimental data, and further motivates the use of an alternate paradigm to describe fusion reactions.

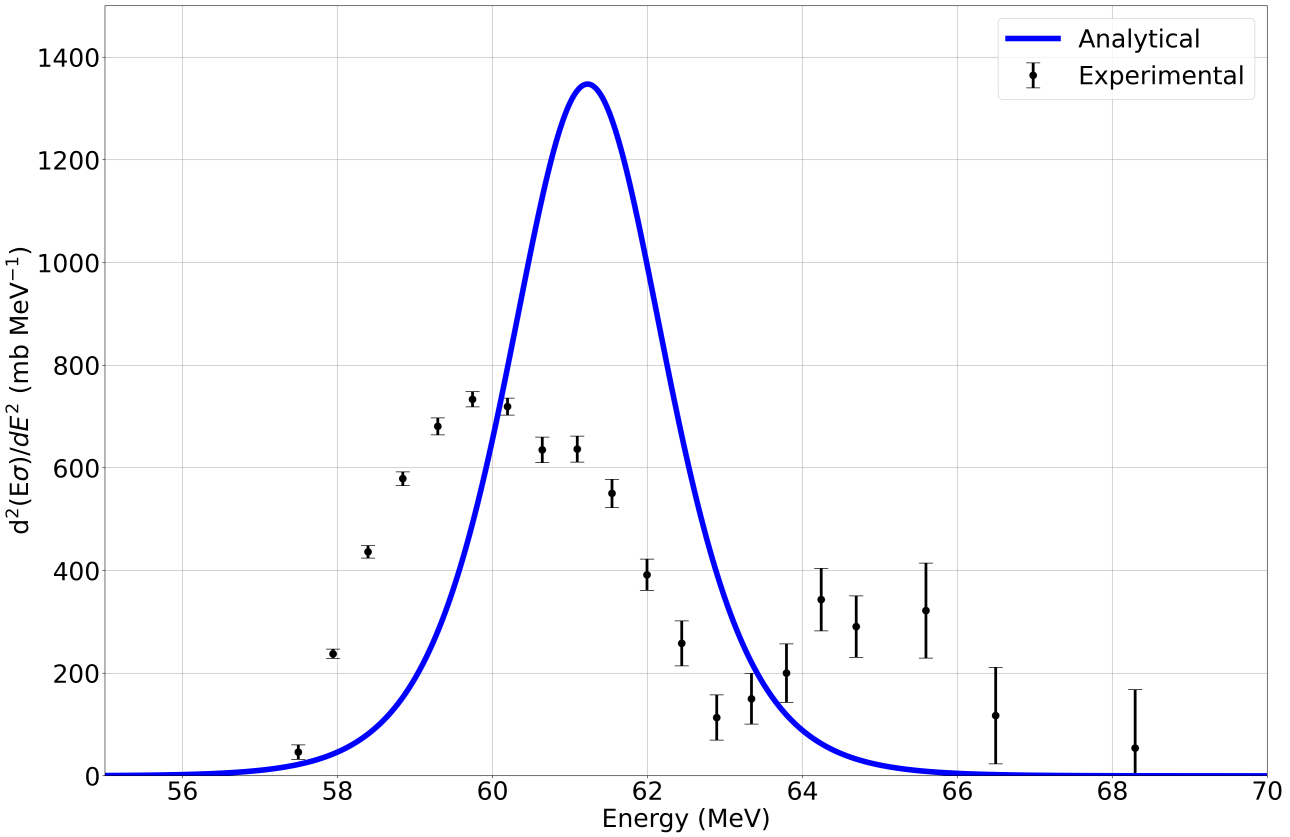

Figure 3: Barrier Distribution for a $\ell = 0$ $^{144}Sm + ^{16}O$ fusion scenario. Black: Experimental data with error bars [16]. Blue: Analytical formula (equation 12).

3 Computational Methods

3.1 Finite Difference Approximation

The time dependent Schrödinger equation,

$$i\hbar\frac{\partial}{\partial t}\Psi(x,t) = -\frac{\hbar^2}{2m}\frac{\partial^2}{\partial x^2}\Psi(x,t) + V(x)\Psi(x,t), \tag{15}$$

can be solved using finite difference approximations, specifically the approximation exploited was an explicit, forward Euler method, for solving partial differential equations. The single spatial and temporal dimensions are discretized onto grids, with finite separation between grid points of Δx and Δt respectively. The wavefunction can now be rewritten in the form Ψ_j^m, where j is the index for the spatial grid, and m is the index for temporal grid. The first order derivatives can be extracted directly from first principles of calculus, and the second order derivative can be found using a Taylor expansion about a point x, ignoring higher order terms. These approximations can be used to rewrite (15),

$$i\hbar\left(\frac{\Psi_j^{m+1} - \Psi_j^m}{\Delta t}\right) = -\frac{\hbar^2}{2m}\left(\frac{\Psi_{j+1}^m - 2\Psi_j^m + \Psi_{j-1}^m}{\Delta x^2}\right) + V_j^m\Psi_j^m, \tag{16}$$

which crucially involves a term for the wavefunction at the next step in time Ψ_j^{m+1}. Rearranging for this term gives,

$$\Psi_j^{m+1} = \Psi_j^m + \frac{i\hbar}{2m}\frac{\Delta t}{\Delta x^2}\left(\Psi_{j+1}^m - 2\Psi_j^m + \Psi_{j-1}^m\right) - \frac{i\Delta t}{\hbar}V_j^m\Psi_j^m, \tag{17}$$

which can be solved numerically, and is used to propagate a known initial wavefunction in time. Importantly, the quantity $\Delta t/\Delta x^2$ must be sufficiently small to ensure numerical stability and prevent rapid solution divergence. The spatial grid was discretized with 1200 steps, and constructed to capture the natural scale in which the Coulomb barrier and potential pocket forms seen in Fig. 1. Nuclear fusion reaction dynamics occur on a natural timescale of 10^{-22} seconds. The discretized temporal grid is therefore constructed from an initial time of $t = 0$ to $t = 60 \times 10^{-22}$ seconds. To ensure the numerical stability condition was satisfied, a $\Delta t = 10^{-29}$ seconds was implemented, yielding 6×10^8 time steps per simulation. The Python programme requires a 2-D array of shape $1200 \times \left(6 \times 10^8\right)$ with 7.2×10^{11} individual 64-float data values to be initialized and then populated with the wavefunction solution. Consequently, each simulation would require a large amount of storage for this 2-D array, which was not available on the my home desktop computer. To combat this issue, I retrofitted a step-skipping scheme, introduced to me during my placement year, where I ran an advanced scientific code, DREAM [25], which operated said scheme for its simulations. I still used a time step of $\Delta t = 10^{-29}$ s, to numerically solve the TDSE, but instead of saving every time step, I saved the wavefunction solution every 10000 time steps, producing a much smaller and storage friendly 2-D array of 7.2×10^7 data points.

3.2 Absorption Potential

An absorption potential is imposed to encapsulate the effect of the fusion process within the Coulomb barrier. The imaginary potential,

$$W(r) = -\frac{W_0}{1 + \exp\left[\frac{r - R_{pocket}}{a_W}\right]}, \tag{18}$$

is of the form of a Woods-Saxon potential, with R_{pocket} being the location within the Coulomb barrier where the potential is minimised. The potential "leads to loss of flux of the collective motion, and the potential physically represents degrees of freedom not accounted for in the Hamiltonian, such as complex non-collective excitations in the compound nucleus" [17]. Including the real potential (seen in Fig. 1), for a head-on $\ell = 0$ collision, the total potential and final potential incorporated within the simulations becomes,

$$V(r) = V_N(r) + V_C(r) + iW(r). \tag{19}$$

3.3 Wavefunction

The radial motion of the $^{16}O-^{144}Sm$ is represented by a GWP wavefunction supplied to the TDSE and propagated on the radial spatial grid r, and time temporal grid, t. The initial wavefunction includes a imaginary exponential term that provides the wave packet with boost towards $r = 0$,

$$\psi_0(r) = N^{-1} \exp\left(-\frac{(r-r_0)^2}{2\sigma_0^2}\right) \exp(-ik_0 r). \tag{20}$$

r_0 is the initial position of centroid and σ_0 is the spatial width of the wave packet. The initial wavefunction must be equal to zero at the boundaries of the spatial grid, $\psi_0(r=0) = \psi_0(r=\infty) = 0$, and must be normalised yielding a normalisation coefficient, N, from,

$$N^2 \langle \psi_{t=0} | \psi_{t=0} \rangle = 1. \tag{21}$$

Finally, k_0 is the mean wavenumber of the GWP which can be found by solving,

$$E_0 = \langle \psi_{t=0} | \hat{H} | \psi_{t=0} \rangle. \tag{22}$$

For a given initial incident mean energy E_0 and initial Gaussian spatial width σ_0, equation (22) can be rewritten as,

$$E_0 = \frac{\hbar^2 k_0^2}{2\mu} + \langle \psi_{t=0} | V_C(r) | \psi_{t=0} \rangle + \frac{\hbar^2}{2\mu\sigma_0^2}. \tag{23}$$

k_0 can be found via rearranging and solving equation (23) and importantly, the last term of equation (23) describes the fluctuation energy of the GWP due to its finite energy variance.

3.4 Simulation Parameters

The simulation programme was written in Python 3.11 ab inito[1] for my investigation, and the the full simulation code can be found in **Appendix B**. A variety of supporting libraries were imported, including but not limited to: *Matplotlib* for static and animated graphical visualizations, *Numpy* for various mathematical tools and optimizations, *SciPy* for scientific algorithms and constants, *Pandas* for data structures utility and analysis, and finally, *Numba*, for code compilation techniques. Scientific codes have a strong tendency to quickly become computationally demanding with regard to data storage and CPU usage. Often, simulation codes are compiled and externally executed on High Powered Computing (HPC) clusters, purpose built for computationally expensive simulations. Simulations for this investigation were run on the author's home computer necessitating the use of an advanced code compiler, Numba jit [26], to translate the Python script into machine code for drastically reduced computation times. Each Simulation took approximately 70 minutes on a Windows 11, 16GB RAM, Intel(R) Core(TM) i7-10700KF CPU @ 3.8 GHz and a Nvidia GeForce RTX 3060 personal desktop computer. Two sample scripts simulating quantum tunneling were accessed and used for inspirational purposes[2]. Overall, 112 individual simulations were conducted with an average clock time of 72 minutes for a total run time of 8064 minutes, or approximately 5.5 days of computation time.

Variable	Value	Description
Δr (fm)	0.1	Step length of the single spatial dimension radial grid
r_{min} (fm)	0	Minimum value of radial grid
r_{max} (fm)	120	Maximum value of radial grid
Δt (s)	1×10^{-29}	Simulation time step for wavefunction propagation
t_{min} (s)	0	Minimum value of time grid and simulation start time
t_{max} (s)	60×10^{-22}	Maximum value of time grid and simulation end time
A_P	16	Projectile nucleon number (Oxygen)
A_T	144	Target nucleon number (Samarium)
ℓ	0	Orbital Angular Momentum
V_{WS} (MeV)	105.1	Wood-Saxon maximum potential depth
r_{WS} (fm)	1.1	Wood-Saxon well center factor
a_{WS} (fm)	0.75	Wood-Saxon well diffuseness
B (MeV)	61.2	Maximum height of Coulomb Barrier
r_0 (fm)	10.8	Radius of the maximum height of the Coulomb barrier
$\hbar\omega$ (MeV)	4.28	Curvature of Coulomb barrier
W_0 (MeV)	50	Absorption well maximum potential depth
R_0 (fm)	7.01	Radius at which the real potential is minimised
a_W (fm)	0.2	Absorption well diffuseness
r_0 (fm)	70	Initial radius of the GWP centroid

Table 1: General and simulation parameters used in this study.

[1] Code was written from the inception of the final year project and was fully written by the author of this report, with no additional authors or initial scripts provided.

[2] The first script by 'louishrm' accessible via Github [27], the second script by 'lukepolson' accessible via Github [28].

3.5 Transmission Probability

The probability of the GWP transmitting through the barrier, and therefore the probability of the projectile fusing with the target, can be found from,

$$P_{fus} = 1 - \langle \psi_{r,t=\infty} | \psi_{r,t=\infty} \rangle. \tag{24}$$

Quantum mechanics enforces that wavefunctions must be normalizable to unity, to properly and fully describe a system. This propagates through to the Schrödinger equation, where the Hamiltonian operator is a unitary operator. Being unitary, if the system is known in particular state, it can be solved using the TDSE for any future time, and in principle, any previous time as there is no loss of information. However, to include the process of fusion within the simulation, an extra complex potential from equation (18) is imposed. The Hamiltonian of the system is now non-Hermitian where, if the GWP occupies the potential pocket, it will be captured by the imaginary absorption potential and the normalisation coefficient of the wavefunction will be reduced. Equation (24) calculates the difference in normalisation coefficient at $t = 0$ and $t = \infty$, which quantifies the probability of fusion occurring for the simulated system. Following the wave packet interaction with the Coulomb barrier, the remaining wavefunction probability density of the GWP is reflected away from the origin. After a sufficiently long period of time post-reflection, the normalisation coefficient of the wavefunction plateaus. Therefore, the probability of transmission can be found at an earlier finite time instead of at $t = \infty$. Preliminary simulations were carried out, where 60×10^{-22} s was found to be a suitable simulation length to acquire a plateaued coefficient, which influenced simulation time for the main study.

4 Results and Discussion

4.1 Probability of Fusion

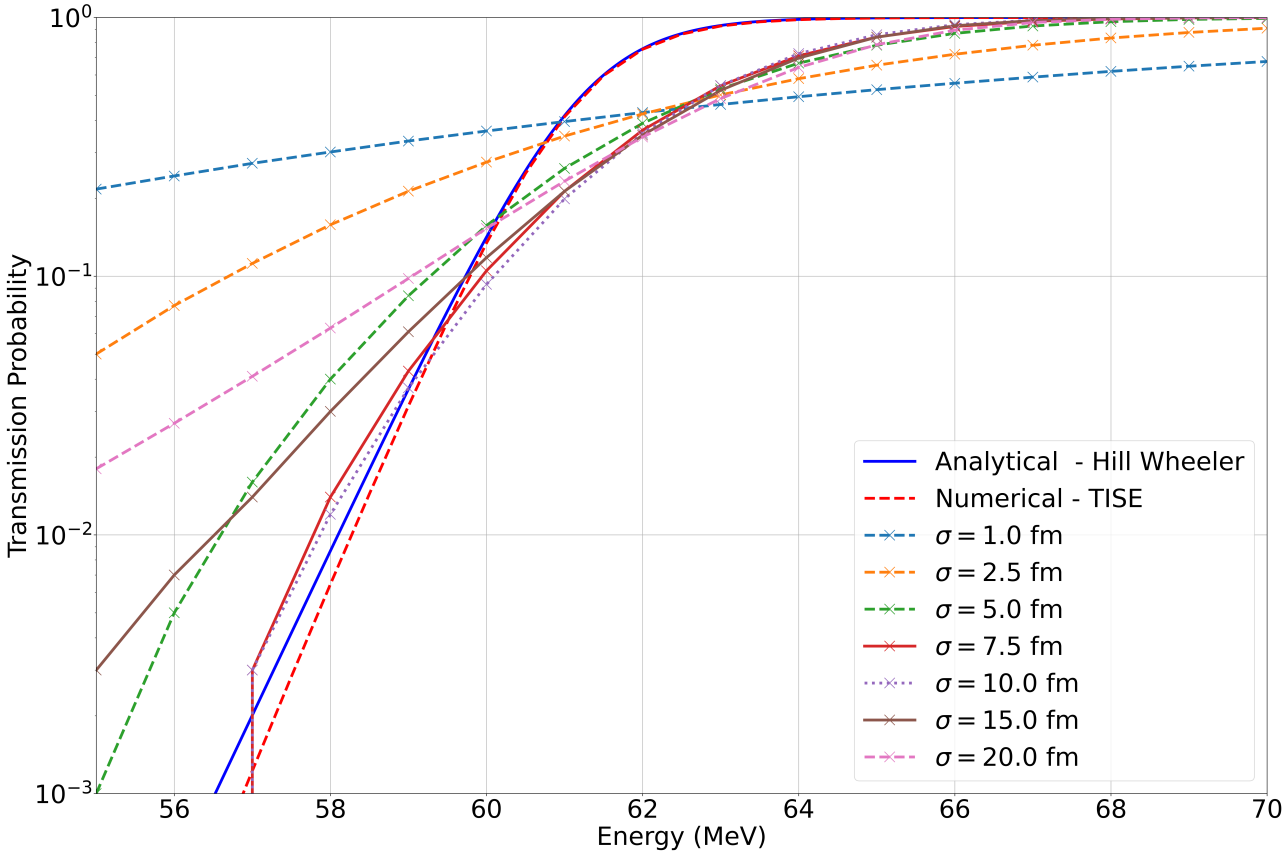

Figure 4: TDSE GWP simulations of a $\ell = 0$ $^{144}Sm + ^{16}O$ fusion reaction with varying initial gaussian spatial widths, σ_0 . Analytical Hill-Wheeler formula and Time Independent Schrödinger Equation (TISE) solution are plotted for comparison.

For the $\ell = 0$ $^{144}Sm + ^{16}O$ fusion reaction, a simulation study was conducted over an array of initial Gaussian spatial widths, $1 \leq \sigma_0 \leq 20$ fm, and initial energies, $55 \leq E_0 \leq 70$ MeV, in which the results of this study is plotted in figure 4. The relative difference of the GWP simulation transmission probabilities to the analytical Hill-Wheeler transmission probabilities is also plotted in Fig. 5 for further analysis. It was found that, as sigma increases from $\sigma_0 = 1$ fm to $\sigma_0 = 10$ fm, the TDSE simulation solutions for the transmission probabilities tended towards both the analytical and TISE solutions, with the relative difference, at a particular energy, decreasing as well. Further, $\sigma_0 = 10$ fm was found to offer the most accurate transmission probabilities, on average, across all energies, where it importantly yielded the lowest relative difference at sub-barrier energies ($E < 61.2$ MeV) in comparison to all other values of σ_0 (by orders of magnitude). Interestingly, the $\sigma_0 = 15$ and 20 fm simulations produced less accurate results for the transmission probabilities compared to other values of σ_0, most significantly in comparison to $\sigma_0 = 10$ fm. The size of the radial grid is likely the cause of the divergence, with the initial spatial widths of the GWP becoming significant in comparison to the span of the grid. This is supported by similar studies simulating smaller gaussian spatial widths, $\sigma_0 = 3$ fm and $\sigma_0 = 10$ fm, on spatial grids which span significantly larger distances, $r_{max} = 350$ fm [19] and $r_{max} = 500$ fm [17] respectively. Lastly, the GWP simulation transmission probabilities showed increasing accuracy at higher values of energy, and a convergence point for transmission probabilities, for all σ_0, around $E_0 \approx 62$ MeV.

Importantly, using a GWP initial wavefunction gives rise to a systematic error relating to the GWP exhibiting a distribution of energies. Conversely, experimental fusion reactants have definite and strong peaks in their energy distributions with regard to their radial motion. Consequently, this energy distribution contributes in an

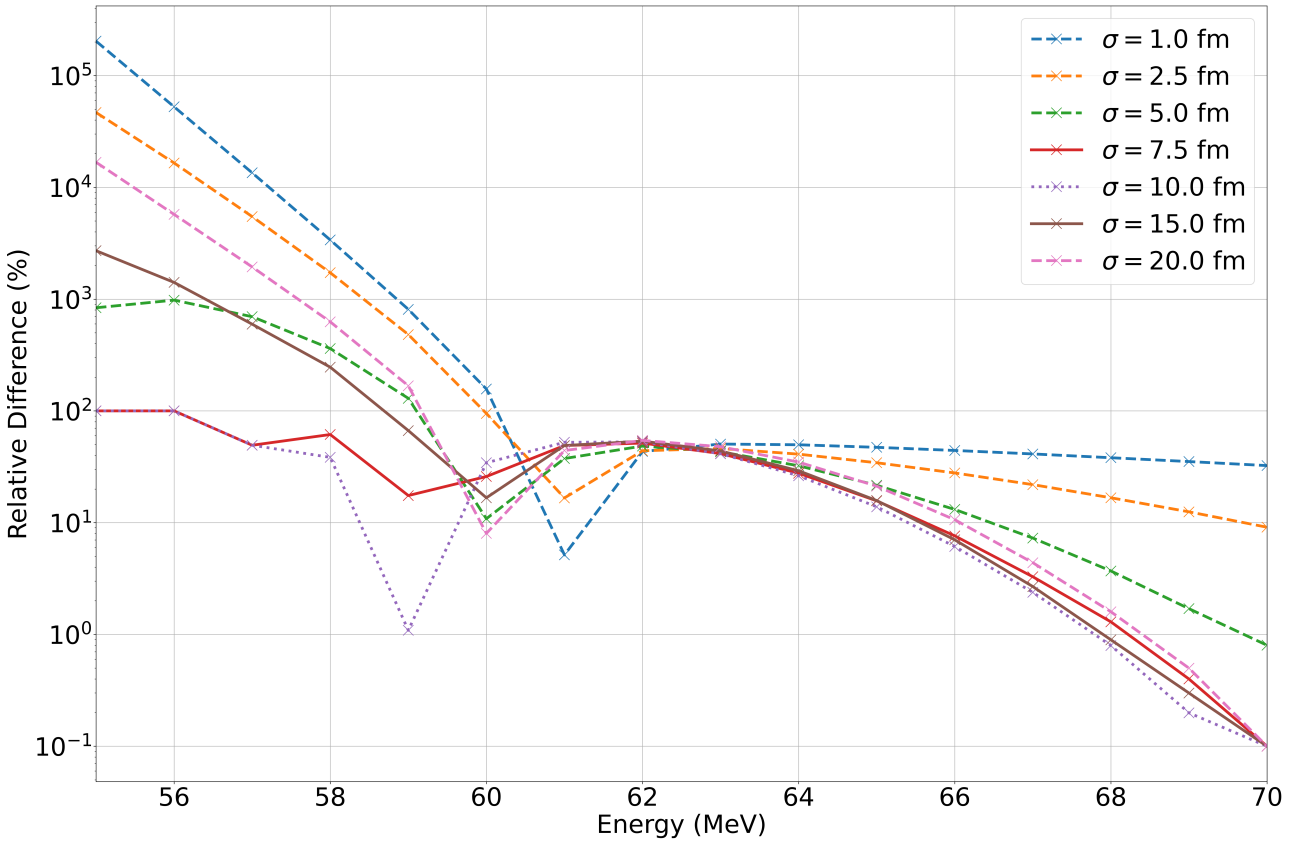

Figure 5: Relative difference of simulation transmission probabilities to analytical Hill Wheeler transmission probabilities as a function of initial GWP energy E_0 and for various initial Gaussian spatial widths σ_0.

un-realistic manner to the numerically calculated transmission probabilities, as energies around but unequal to the prescribed E_0 produce varying transmission probabilities. To resolve this, there is a numerical method to extract energy-resolved transmission properties with a set of user-inputted fitting parameters. The *Window Operator Method* provides this utility and has been shown in multiple other GWP simulations to successfully resolve in energy the transmission coefficient [17, 19, 18, 20]. It should be noted that these studies involved simulations using the coupled channel formalism, rather than the single barrier model. However, the viability of the *Window Operator Method* to resolve the simulated transmission probabilities is unaffected by the model used within the simulations (single barrier or coupled channel), such that the method can be applied to this study using the single barrier model. Time constraints prevented successful application of the method within this study, but it would be a vital next step for future investigations.

4.2 Numerical Methods

The finite difference approximation is a useful numerical tool owing to its simple implementation and grounded derivation from first principles. It has been found that choosing a Δt and Δx such that $\Delta t/\Delta x^2$ is sufficiently small, prevents rapid divergence of the solution and enables the method to be used for numerical simulations. However, a more rigorous evaluation of the forward Euler method sees an inherent unconditionally instability regardless of $\Delta t/\Delta x^2$ being minimised [29]. This unconditionally instability likely manifests within the non-constant normalisation coefficient during the simulations. Similar GWP fusion reaction studies, see a plateauing normalisation coefficient following the packet interaction and/or reflection with the Coulomb barrier, see reference [17] Fig 4. However, the normalisation coefficient of my simulations saw a steady reduction post-interaction, likely attributable to this unconditional instability of the numerical method. The difference between the maximum value for the coefficient and final value following this reduction, was analysed to assess the impact on the results. The evolution of the probability of fusion for an exemplar simulation is presented in Fig. 6, highlighting the non-zero but very small loss of normalisation post Coulomb barrier interaction of the GWP. Across the

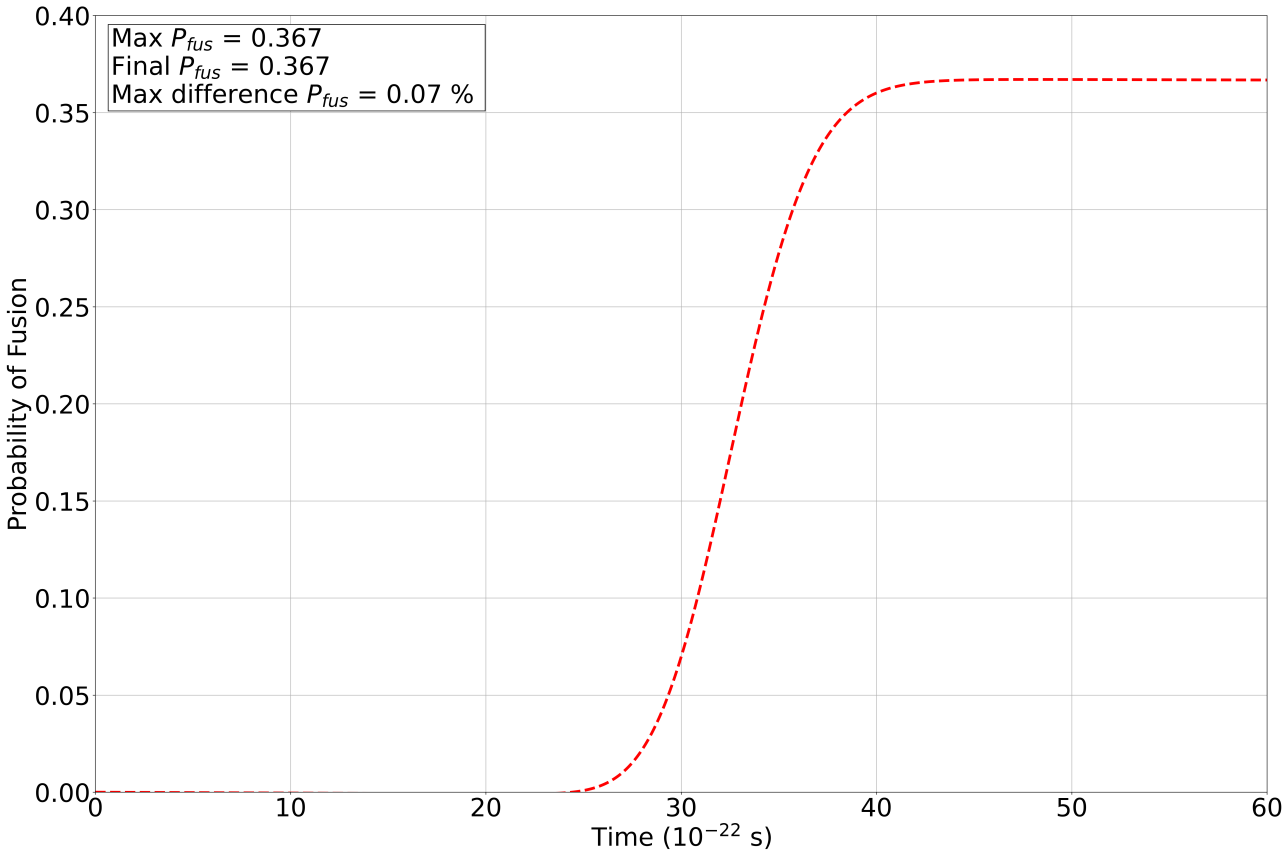

Figure 6: Evolution of the fusion probability parameter during a simulation ($\sigma_0 = 7.5$ fm, $E_0 = 62$ MeV). The maximum value, final value and percentage difference between the maximum and final value, for the probability of fusion is displayed as text.

simulations, with varying input parameters σ_0 and E_0, the relative difference was found to be always below 0.1%. Ergo, it is fair to say that the impact of this reduction in normalisation due to the possible numerical instability appears to be a non-significant source of error.

Various other numerical methods are available as alternatives to the forward Euler finite difference approximation used in this study. The Crank-Nicholson implicit method is an improved finite difference approximation which critically, is one of the few primary numerical methods displaying unconditionally numerical stability regardless of the $\Delta t/\Delta x^2$ used [29]. This method can be executed via the construction of Padé matrices, which can be solved via matrix mechanics for vastly superior computation speeds and reduced storage requirements [30]. An attempt to exploit this method was made to use as a comparison to the Euler method, but coding issues and time constraints prevented successful implementation. The TDSE is an eigenvalue problem equation which enables the non-numerical technique of determining the eigenstate evolution of the wavefunction, as another alternative method to produce computational simulations [28]. It would be paramount for future GWP nuclear fusion investigations to explore the use of such alternate methods for comparative purposes and reaffirm the accuracy of results that are obtained.

4.3 Wavefunction Selection

Representing the radial motion of the $^{16}O - ^{144}Sm$ as a GWP has a multitude of advantages. Firstly, GWPs are naturally solutions of wave equations, where in the context of quantum mechanics, the GWP is a dispersive solution to the TDSE wave equation. As a mathematical function, GWPs are simple, contain adjustable parameters, and are symmetric. These properties make them applicable in a wide range of scenarios, as well as enabling them to simplify any calculations or solutions they are used within. The nature of quantum mechanics gives rise to probabilistic descriptions of systems and structures, namely particles and compound nuclei. GWPs are innately

probabilistic with key properties such as energy, position and momentum being indefinite and described by distributions. Consequently, Fourier transforming a GWP's position distribution will produce another Gaussian distribution. Importantly, this ensures that Heisenberg's Uncertainty Principle (HUP), a core tenant of quantum mechanics, is always satisfied ($\Delta x \Delta p \geq \hbar/2$). For a GWP with minimised uncertainty, HUP's inequality becomes equality being perfectly satisfied, $\Delta x \Delta p = \hbar/2$. GWPs exhibit an array of aforementioned de-localised features e.g. position distribution, in addition to a number of localised features vital for satisfying specific scenario and quantum physics constraints. GWPs can be constrained to a finite region of space, with a fixed central amplitude and a deterministic trajectory-based description of the wave packets motion through space [31].

Whilst a GWP may seem like a strong candidate for the initial wavefunction, several drawbacks of GWPs do exist and must be addressed in the context of reaction and scenario this study investigates. Firstly, GWPs can undergo adverse evolution near the boundaries of systems or when in the presence of excessively large or strongly non-quadratic potentials. Over sufficiently long periods of time, GWPs can become very spatially dispersed and a poor representation of systems such as nuclei. Lastly, the radial velocity, and therefore energy, of an inbound ^{16}O nuclei experimentally, is a very finite and definite variable whereas the simulated GWP contradictorily, externalizes a distribution of energies with an expectation value equivalent to the classical experimental value. Within the simulations, the GWP never went near the spatial boundaries $r \approx 0,120 fm$, and experienced a potential slowly varying in r, with the Coulomb barrier being highly quadratic-like and of similar energy to that of the GWP, $E_0 \approx B \approx 60$ MeV. Further, the simulations are run for 60×10^{-22} seconds, a relatively short period of time, where dispersive effects should not materialize and strongly impact the viability of the wavefunction to represent the radial motion of the $^{16}O - ^{144}Sm$. The disconnect between the projectile ^{16}O finite experimental value and distribution of values within the simulations is highlighted in section 4.1, and a resolution to this problem can be found with the also mentioned *Window Operator Method*. There do exist other possible functions to represent the initial wavefunction, however, considering the symmetries of the system, the boundary conditions and scenario at hand, the GWP ansatz is the most viable option available.

5 Conclusions

Implementing a finite difference approximation for the TDSE, and, representing the radial motion of the $^{16}O - ^{144}Sm$ as a GWP, I successfully simulated a head-on nuclear fusion reaction, utilising a single barrier model, with a selection of phenomenological parameters. A simulation scan over an energy range of $55 \leq \sigma_0 \leq 70$ MeV, provided an array of useful transmission probability data covering low fusion scenarios $P_{fus} \approx 0.01$ to maximal fusion reactions with $P_{fus} \approx 1$. Analysing GWP's, with a variety of initial spatial widths illustrates certain drawbacks of using wave packets to represent systems (nuclei), where disconnections in the energy profile of the ^{16}O projectile arise between simulation and experimental results. A number of sources of error have been identified, which potentially degrade the accuracy of the simulations. The key sources include: GWP energy distribution and dispersive properties, viability of the forward Euler finite difference approximation as a numerically stable method, numerous parameters that are fitted from experimental data or from approximations. The single barrier model for fusion has been proven to be a dissatisfactory framework to explain low energy sub-barrier fusion with experimental nuclear fusion cross section data discrepancies [12] and data inversion techniques which highlight a divergence in the reactions effective potential [5]. Subsequent research should be focused on utilising and analysing the viability of the improved coupled channel formalism model for fusion reactions, with a number of possible additional avenues of study e.g. looking at non-head-on collisions with $\ell \neq 0$. Implementing a variety of alternative methods in addition to the forward Euler finite difference approximation e.g. Crank-Nicholson finite implicit and Eigenvalue evolution methods, to numerically solve the TDSE will enable a rigorous comparison and assessment of the validity of the simulation results. It would also be paramount to exploit energy projection methods such as the, *Window Operator Method*, to resolve the impact of the GWP's innate energy distribution on the transmission probability results. Lastly, exploring fusion reactions with different reactants would equally be tantamount to ensure the cohesion of the simulation methods and theoretical models used across scenarios. This would facilitate the possibility for supplemental investigations such as, probing how nuclei with different nucleon numbers affects the interaction. A supplemental investigation based upon this would be favorable due to the wealth supporting experimental data, such as for $^{16}O + ^{144}Sm, ^{148}Sm, ^{154}Sm$ [16].

6 Acknowledgements

I would like to extend my thanks to Dr. Alexis Diaz Torres, for his continual support during my investigation, assisting with invaluable insight, and exposition into the theory of nuclear fusion.

References

[1] R. D. E. Atkinson and F. G. Houtermans. “Zur Frage der Aufbaumöglichkeit der Elemente in Sternen”. In: *Zeitschrift fur Physik* 54.9-10 (Sept. 1929), pp. 656–665. DOI: 10.1007/BF01341595.

[2] The Atomic Archive. *"Mike" Device is Tested*. Online. Date Accessed: 7 April 2024. URL: https://www.atomicarchive.com/history/hydrogen-bomb/page-13.html.

[3] ITER. *WHAT IS ITER?* Online. Date Accessed: 7 April 2024. URL: https://www.iter.org/proj/inafewlines.

[4] J. J. (Jun John) Sakurai and Jim Napolitano. *Modern quantum mechanics*. eng. Second edition. Cambridge, United Kingdom: Cambridge University Press, 2017. ISBN: 9781108422413.

[5] A. B. Balantekin and N. Takigawa. “Quantum tunneling in nuclear fusion”. In: *Rev. Mod. Phys.* 70 (1 1998), pp. 77–100. DOI: 10.1103/RevModPhys.70.77. URL: https://link.aps.org/doi/10.1103/RevModPhys.70.77.

[6] H. A. Bethe. “Energy Production in Stars”. In: *Phys. Rev.* 55 (5 1939), pp. 434–456. DOI: 10.1103/PhysRev.55.434. URL: https://link.aps.org/doi/10.1103/PhysRev.55.434.

[7] J.R. Birkelund et al. “Heavy-ion fusion: Comparison of experimental data with classical trajectory models”. In: *Physics Reports* 56.3 (1979), pp. 107–166. ISSN: 0370-1573. DOI: https://doi.org/10.1016/0370-1573(79)90093-0. URL: https://www.sciencedirect.com/science/article/pii/0370157379900930.

[8] R. Bass. “Fusion of heavy nuclei in a classical model”. In: *Nuclear Physics A* 231.1 (1974), pp. 45–63. ISSN: 0375-9474. DOI: https://doi.org/10.1016/0375-9474(74)90292-9. URL: https://www.sciencedirect.com/science/article/pii/0375947474902929.

[9] Roger D. Woods and David S. Saxon. “Diffuse Surface Optical Model for Nucleon-Nuclei Scattering”. In: *Phys. Rev.* 95 (2 1954), pp. 577–578. DOI: 10.1103/PhysRev.95.577. URL: https://link.aps.org/doi/10.1103/PhysRev.95.577.

[10] David Lawrence Hill and John Archibald Wheeler. “Nuclear Constitution and the Interpretation of Fission Phenomena”. In: *Phys. Rev.* 89 (5 1953), pp. 1102–1145. DOI: 10.1103/PhysRev.89.1102. URL: https://link.aps.org/doi/10.1103/PhysRev.89.1102.

[11] Louis C. Vaz, John M. Alexander, and G.R. Satchler. “Fusion barriers, empirical and theoretical: Evidence for dynamic deformation in subbarrier fusion”. In: *Physics Reports* 69.5 (1981), pp. 373–399. ISSN: 0370-1573. DOI: https://doi.org/10.1016/0370-1573(81)90094-6. URL: https://www.sciencedirect.com/science/article/pii/0370157381900946.

[12] M Beckerman. “Sub-barrier fusion of two nuclei”. In: *Reports on Progress in Physics* 51.8 (1988), p. 1047. DOI: 10.1088/0034-4885/51/8/001. URL: https://dx.doi.org/10.1088/0034-4885/51/8/001.

[13] A. B. Balantekin, S. E. Koonin, and J. W. Negele. “Inversion formula for the internucleus potential using sub-barrier fusion cross sections”. In: *Phys. Rev. C* 28 (4 1983), pp. 1565–1569. DOI: 10.1103/PhysRevC.28.1565. URL: https://link.aps.org/doi/10.1103/PhysRevC.28.1565.

[14] W Reisdorf. “Heavy-ion reactions close to the Coulomb barrier”. In: *Journal of Physics G: Nuclear and Particle Physics* 20.9 (1994), p. 1297. DOI: 10.1088/0954-3899/20/9/004. URL: https://dx.doi.org/10.1088/0954-3899/20/9/004.

[15] M. Dasgupta et al. “MEASURING BARRIERS TO FUSION”. In: *Annual Review of Nuclear and Particle Science* 48.Volume 48, 1998 (1998), pp. 401–461. ISSN: 1545-4134. DOI: https://doi.org/10.1146/annurev.nucl.48.1.401. URL: https://www.annualreviews.org/content/journals/10.1146/annurev.nucl.48.1.401.

[16] J. R. Leigh et al. "Barrier distributions from the fusion of oxygen ions with ^{144,148,154}Sm and ^{186}W". In: *Phys. Rev. C* 52 (6 1995), pp. 3151–3166. DOI: 10.1103/PhysRevC.52.3151. URL: https://link.aps.org/doi/10.1103/PhysRevC.52.3151.

[17] Terence Vockerodt and Alexis Diaz-Torres. "Describing heavy-ion fusion with quantum coupled-channels wave-packet dynamics". In: *Phys. Rev. C* 100 (3 2019), p. 034606. DOI: 10.1103/PhysRevC.100.034606. URL: https://link.aps.org/doi/10.1103/PhysRevC.100.034606.

[18] TERENCE VOCKERODT. "Quantum dynamics of heavy-ion collisions at Coulomb energies using the time-dependent coupled-channel wave-packet method". PhD thesis. University of Surrey, 2021. DOI: 10.15126/thesis.900012.

[19] Terence Vockerodt and Alexis Diaz-Torres. "Calculating the *S*-matrix of low-energy heavy-ion collisions using quantum coupled-channels wave-packet dynamics". In: *Phys. Rev. C* 104 (6 2021), p. 064601. DOI: 10.1103/PhysRevC.104.064601. URL: https://link.aps.org/doi/10.1103/PhysRevC.104.064601.

[20] Maddalena Boselli and Alexis Diaz-Torres. "Quantifying low-energy fusion dynamics of weakly bound nuclei from a time-dependent quantum perspective". In: *Phys. Rev. C* 92 (4 2015), p. 044610. DOI: 10.1103/PhysRevC.92.044610. URL: https://link.aps.org/doi/10.1103/PhysRevC.92.044610.

[21] C. Y. Wong. "Interaction Barrier in Charged-Particle Nuclear Reactions". In: *Phys. Rev. Lett.* 31 (12 1973), pp. 766–769. DOI: 10.1103/PhysRevLett.31.766. URL: https://link.aps.org/doi/10.1103/PhysRevLett.31.766.

[22] A.C Berriman et al. *Barriers to Fusion*. Online. Date Accessed: 8/4/2024. URL: https://inis.iaea.org/collection/NCLCollectionStore/_Public/31/033/31033889.pdf.

[23] E Piasecki, L. Swiderski, and J Jastrzebski. *Fusion Barrier distributions*. Online. Date Accessed: 8/4/2024. 2007. URL: https://inis.iaea.org/collection/NCLCollectionStore/_Public/38/068/38068150.pdf.

[24] N. Rowley, G.R. Satchler, and P.H. Stelson. "On the "distribution of barriers" interpretation of heavy-ion fusion". In: *Physics Letters B* 254.1 (1991), pp. 25–29. ISSN: 0370-2693. DOI: https://doi.org/10.1016/0370-2693(91)90389-8. URL: https://www.sciencedirect.com/science/article/pii/0370269391903898.

[25] Chalmers Plasma Theory Group Mathias Hoppe Ola Embreus. *Disruption and Runaway Electron Analysis Model*. Online, Github. 2021. URL: https://ft.nephy.chalmers.se/dream/.

[26] Inc Anaconda. *Compilling code with @jit*. Online, Github. URL: https://numba.pydata.org/numba-doc/latest/user/jit.html.

[27] louishrm. *Quantum-tunneling / QM Tunneling.ipynb*. Github Online. 2022. URL: https://github.com/louishrm/Quantum-Tunneling/blob/main/QM%20Tunnelling.ipynb.

[28] Lukepolson. *Python Metaphysics series / vid17.ipynb*. Github Online. 2021. URL: https://github.com/lukepolson/youtube_channel/blob/main/Python%20Metaphysics%20Series/vid17.ipynb.

[29] Randall LeVeque. *Finite Difference Methods for Ordinary and Partial Differential Equations Steady-State and Time-Dependent Problems*. Society for Industrial and Applied Mathematics, 2007. DOI: http://dx.doi.org/10.1137/1.9780898717839. URL: https://tevza.org/home/course/modelling-II_2016/books/Leveque%20-%20Finite%20Difference%20Methods.pdf.

[30] James Lenton, Iain Lee, and Alexis Diaz-Torres. "Quantum dynamics of a nucleon in the Fermi accelerator". In: *Annals of Physics* 434 (2021), p. 168624. ISSN: 0003-4916. DOI: https://doi.org/10.1016/j.aop.2021.168624. URL: https://www.sciencedirect.com/science/article/pii/S000349162100230X.

[31] David Tannor. *Introduction to Quantum Mechanics a time dependent perspective*. Ed. by Lee Young. University Science Books, 2007.

A Animations

A useful simulation assessment and debugging tool was to animate the propagation of the GWP. Each Simulation conducted had an associated animation of its real wavefunction and probability density function. I have created a selection of animations from simulations for visual aid. These have been uploaded to my youtube channel:

`https://www.youtube.com/channel/UCcW15N-NkN4qj1uIWBAafqg`.

Following list of simulations have been animated and uploaded to the youtube channel.

- $E_0 = 59$ MeV, $\sigma_0 = 10$ fm
- $E_0 = 62$ MeV, $\sigma_0 = 10$ fm
- $E_0 = 68$ MeV, $\sigma_0 = 10$ fm
- $E_0 = 62$ MeV, $\sigma_0 = 10$ fm, Probability Density Function
- $E_0 = 62$ MeV, $\sigma_0 = 1$ fm
- $E_0 = 62$ MeV, $\sigma_0 = 20$ fm

B Code

Code used for for this report can be found in my GitHub repository:

`https://github.com/dp0768/FYP.git`